INELASTIC LIGHT SCATTERING

BY LARGE STRUCTURED PARTICLES

BRUCE J. BERNE *and* RALPH NOSSAL

From the Department of Chemistry, Columbia University, New York 10027, and the Physical Sciences Laboratory, Division of Computer Research and Technology, National Institutes of Health, Bethesda, Maryland 20014

ABSTRACT Autocorrelation functions are computed for nonspherical particles whose dimensions are comparable to or greater than the wavelength of scattered light. Particular attention is given to models of motile microorganisms. Results for Gaussian ellipsoids, finite thin rods, ellipsoids with internal structures, and dumbbell-shaped scatterers are derived and compared.

I. INTRODUCTION

Several recent studies have demonstrated the feasibility of using laser inelastic light scattering to obtain kinematic parameters of biological microorganisms. Among these are investigations of the diffusion coefficients of viruses (1–3), the electrophoretic mobilities of erythrocytes (4), and the mean swimming speeds of motile *Escherichia coli* (5, 6).

A major advantage of laser scattering techniques is the rapidity with which measurements are accomplished. Thus, for example, determinations of electrophoretic mobilities of cells can be made in a matter of a few minutes (4). In contrast, classical microelectrophoretic methods require tedious examination of the motion of individual cells. Furthermore, particularly for homogeneous assemblies of scatterers, kinematic parameters oftentimes can be determined with greater precision than with classical methodology. These benefits derive from the large size of the scatterers, since very large amounts of light are scattered by only moderately dense suspensions of such particles. Concomitantly, only minimal effort must be given to cleansing the fluids in which the microorganisms are suspended, since dust and other foreign bodies are comparatively poor scatterers.

For these reasons the large size of the microorganisms make them attractive constituents for study. However, because the dimensions of such particles are similar to or greater than the wavelength of light, they generally cannot be considered merely as point scatterers. Therefore, careful attention must be given to the possible consequences of coherent interference between light scattered from different points of the same particle. With this in mind we investigate the effects of particle structure on the

light scattering spectra for some simple models in the Rayleigh-Gans approximation. Particular regard is given to the derivation of spectra for motile microorganisms.

Our basic model is that of an ellipsoid of revolution, characterized as having a Gaussian mass distribution (Sec. II). This model has the desirable characteristic of being analytically tractable, and spectra (actually, their time transforms) are computed for both motile and diffusing particles (Secs. III, IV). Velocity distributions of the particles are taken to be isotropic. Generally, we assume that motion occurs parallel to the major axes of the particles; effects of off-axial orientation are analyzed in an Appendix. We also analyze variations of the basic model which symbolize internally structured microorganisms. These are, specifically, shell-like (Sec. V) and dumbbell (Sec. VI) models, suggested by "chromatinic bodies" (7, 8) appearing in phase contrast microscope images of bacteria.

Whenever possible, we try to express our results in terms of reduced and normalized variables to facilitate applications to particles and microorganisms of many different sizes. Although references to scatterers having the dimensions and motile characteristics of *E. coli* bacteria frequently occur, we emphasize that our interest in the latter microorganisms derives largely from their role as typifying scatterers of biological origin.

II. SCATTERING FROM AXIALLY SYMMETRIC GAUSSIAN PARTICLES

We consider all particles to be identical and in sufficiently dilute suspension that interparticle interactions and multiple scattering can be neglected. In this case the correlation function $C(Q, t) \sim \langle E_{sc}^*(0) E_{sc}(t) \rangle$ is given in the Rayleigh-Gans approximation as (9, 10)

$$C(Q, t) = \left\langle \sum_{i=1}^{N} \sum_{j=1}^{N} a_i a_j e^{-i\mathbf{Q} \cdot (\mathbf{r}_i(0) - \mathbf{r}_j(t))} \right\rangle, \tag{1}$$

where N, $\{r_i\}$, and $\{a_i\}$ are the total number, the positions, and the excess scattering powers[1] of the distributed scattering centers of a particle. As usual, $Q = 4\pi n \lambda^{-1} \cdot \sin \theta/2$ is the magnitude of the Bragg wave vector. The average $\langle \ldots \rangle$ is taken with respect to the distributions of velocity and orientation of the particles.

In Secs. II–IV we assume that all scattering centers within a particle have equivalent scattering power. Implicitly, we consider internal optical heterogeneities to be describable by spatially variable densities of scattering centers. Equivalently, of course, one could consider the particles to be composed of regions of uniform density but variable polarizability (cf. Secs. V, VI).

The position of the jth scattering center $\mathbf{r}_j(t)$ is $\mathbf{r}_j = \mathbf{R}(t) + \rho_j(t)$, where $\mathbf{R}(t)$ is the center of mass position of the particle and $\rho_j(t)$ is the position of the jth scattering cen-

---

[1]The "excess scattering powers" (E_{sc}) are proportional to the difference between the polarizabilities of the scattering centers and the polarizability of the surrounding medium.

ter relative to the center of mass. Therefore, assuming that all scattering centers have equivalent polarizability, Eq. 1 can be expressed as

$$C(Q, t) = a^2 \left\langle e^{iQ \cdot \Delta R(t)} \sum_j \sum_k e^{-iQ \cdot \rho_j(0)} e^{iQ \cdot \rho_k(t)} \right\rangle , \quad (2)$$

where $\Delta R(t)$ is the displacement of the center of mass at time t. If $P(\rho, t)$ denotes the distribution function for finding a scattering center at ρ at time t, then $NP(\rho, t)d^3\rho$ is the number of centers in $d^3\rho$ at ρ at time t and

$$\sum_{k=1}^{N} e^{iQ \cdot \rho_k(t)} = N \int d^3\rho \, P(\rho, t) e^{iQ \cdot \rho}. \quad (3)$$

We note that $P(\rho, t)$ changes with time only if the particle is nonspherical and is tumbling or experiencing some other axial reorientation. Combining Eqs. 2 and 3 gives

$$C(Q, t) = a_N^2 \left\langle e^{iQ \cdot \Delta R(t)} \int d^3\rho' \int d^3\rho \, P(\rho', 0) P(\rho, t) e^{-iQ \cdot \rho'} e^{iQ \cdot \rho} \right\rangle , \quad (4)$$

where $a_N \equiv Na$ is the total excess polarizability of the particle (the difference between the polarizability of the scattering center and that of the medium in which the particles are suspended).

In the case of a spherical particle, Eq. 4 reduces to

$$C(Q, t) = a_N^2 S(Q) \left\langle e^{iQ \cdot \Delta R(t)} \right\rangle ,$$

where $S(Q)$ is the structure factor for a sphere. However, generally we wish to consider nonspherical particles which have axial symmetry. Therefore, we define $u(t)$ to be a unit vector lying along the major axis of such a particle at time t and further define a body fixed coordinate system (i.e. one that tumbles with the molecule) which has a z axis parallel to $u(t)$ (see Fig. 1).

We next assume that $P(\rho, t)$ is distributed according to a normalized Gaussian distribution in this body fixed frame, viz.,

$$P(\rho, t) = (1/2\pi\sigma_\perp^2)(1/2\pi\sigma_\parallel^2)^{1/2} e^{-z^2/2\sigma_\parallel^2} e^{-(x^2+y^2)/2\sigma_\perp^2}. \quad (5)$$

It follows that

$$\int d^3\rho \, P(\rho, t) e^{iQ \cdot \rho} = e^{-\sigma_\parallel^2 Q_z^2/2} e^{-\sigma_\perp^2 (Q_x^2 + Q_y^2)/2}, \quad (6)$$

where $Q_z = Q \cdot u(t)$. Since $Q_x^2 + Q_y^2 = Q^2 - Q_z^2$, Eq. 6 can be expressed as $\exp[-\frac{1}{2} \cdot (\sigma_\parallel^2 - \sigma_\perp^2)[Q \cdot u(t)]^2] \cdot \exp[-\frac{1}{2}\sigma_\perp^2 Q^2]$, and Eq. 4 becomes

$$C(Q, t) = a_N^2 \exp(-\sigma_\perp^2 Q^2)$$

$$\left\langle \exp(iQ \cdot \Delta R(t)) \exp\left(-\frac{\Delta\sigma^2}{2} Q^2 \{[\hat{Q} \cdot u(0)]^2 + [\hat{Q} \cdot u(t)]^2\}\right) \right\rangle , \quad (7)$$
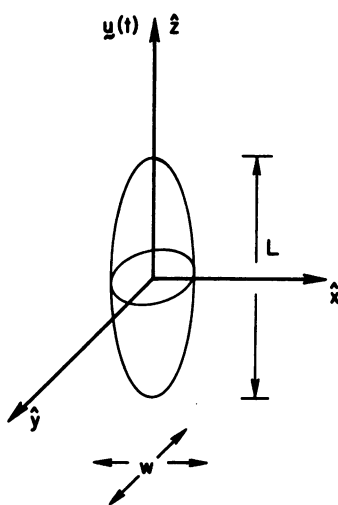
FIGURE 1 Coordinate system defined for ellipsoidal particles (see Eq. 5).

where $\Delta\sigma^2 \equiv \sigma_{\parallel}^2 - \sigma_{\perp}^2$ reflects the deviations from spherical symmetry, and $\hat{Q}$ is a unit vector in the direction of Q. In the following, the model defined to as the Gaussian Particle to distinguish it from other idealized models such as a linear mass distribution or an internally structured particle.

For a spherical particle, $\Delta\sigma^2 = 0$, so that $C(Q, t)$ reduces to $a_N^2 \exp(-\sigma_{\perp}^2 Q^2)\langle \exp \cdot (iQ \cdot \Delta R(t))\rangle$ and contains information related only to translational displacements. On the other hand, if $\Delta\sigma^2 \neq 0$, then $C(Q, t)$ also contains components due to rotational motion.

III. MOTILE MICROORGANISMS

We compute the light-scattering spectrum of motile microorganisms by considering that such particles move in essentially straight-line paths for distances long compared with Q^{-1}. This condition is met to a good degree by various strains of motile *E. coli* bacteria under proper culture conditions and, most probably, it holds for many other motile microorganisms as well (e.g., the flagellated algae *Chlamydomonas* [11]). In this case we can consider the displacement of the particle to be

$$\Delta R(t) = Vt, \qquad (8)$$

where V is the particle velocity.

We now also presume that the particle always moves parallel to its major axis, so that $u(t)$ is independent of time and equal to $\hat{v}$, a unit vector parallel to V (cf. Appendix B). Moreover, in an isotropic environment the velocity distribution function $P(V)$ should not depend on the direction of V. In this event the normalized correla-

tion function $\hat{C}(Q, t) \equiv C(Q, t)/C(Q, 0)$ corresponding to Eq. 7 reduces to

$$\hat{C}_{\text{Ellipsoid}}(Q, t) = \frac{\int_0^\infty dV \int_{-1}^1 \frac{d\eta}{2} e^{iQV t\eta} e^{-\Delta\sigma^2 Q^2\eta^2} W(V)}{\int_{-1}^1 \frac{d\eta}{2} e^{-\Delta\sigma^2 Q^2\eta^2}}, \quad (9)$$

where $\eta \equiv \hat{Q} \cdot \hat{v}$ is the cosine of the angle between V and Q, and $W(V)$ is the speed distribution function $(W(V) = 4\pi V^2 P(V))$. In the limit $\Delta\sigma^2 = 0$ we obtain the result for a spherical particle

$$\hat{C}_{\text{Sphere}}(Q, t) = \int_0^\infty dV j_0(QVt) W(V) = \langle j_0(QVT) \rangle. \quad (10)$$

Since $\hat{C}_{\text{Sphere}}(Q, t)$ is a functional of Qt, Eq. 10 can be inverted to yield the speed distribution $W(V)$ in terms of a Fourier integral of the correlation function (12). However, we remark that, in general, $\hat{C}(Q, t)$ is given as $\hat{C}(Q, t) = \sum_{n=0}^\infty C_{2n}(Q;\sigma) \cdot \langle j_{2n}(QVt) \rangle$ and Eq. 10 is just the first term of an expansion whose higher order terms increasingly important for larger particles and large scattering angles (see Appendix B). Indeed, Eq. 10 is rigorously derivable from Eq. 9 only if $P(\rho)$ is spherically symmetric or the particles small compared with the wavelength of the incident light. The Gaussian model encompassed in Eq. 5 yields analytical solutions for $\hat{C}(Q, t)$ and thus conveniently allows quantitative examination of the manner in which particle anisotrophy causes deviations from Eq. 10; in Appendix A we demonstrate that results obtained from this analytically tractable model are essentially identical to those obtained numerically for a uniformly distributed finite rigid rod, provided that the parameters $\sigma_\parallel$, $\sigma_\perp$ (see Eq. 5) are related to the particle length L and width w according to[2] $\sigma_\parallel = L/\sqrt{10}$, $\sigma_\perp = w/\sqrt{10}$.

In order to complete the calculation, the swimming speed distribution $W(V)$ needs to be specified. For this purpose we take

$$W(V) = 4\pi(\gamma^2/\pi)^{3/2} V^2 e^{-\gamma^2 V^2}, \quad (11)$$

where γ is related to the root mean square (rms) swimming speed $\langle V^2 \rangle^{1/2}$ as

$$\gamma^2 = \frac{3}{2} \langle V^2 \rangle^{-1}. \quad (12)$$

The Gaussian distribution expressed by Eq. 11 is partly conjectural, but it seems to approximate data determined (12) for the swimming speed distribution of motile *E. coli* K12. Fortunately, qualitative aspects of the resulting spectra are not too sensitive to the exact form of $P_s(V)$ (6, 13).

---

[2]Alternatively, e.g., one might demand that 95% of the mass distribution given by Eq. 5 lie within the actual boundaries of the particle. In this case one would obtain $\sigma_\parallel \doteq L/4$, $\sigma_\perp \doteq w/4$.
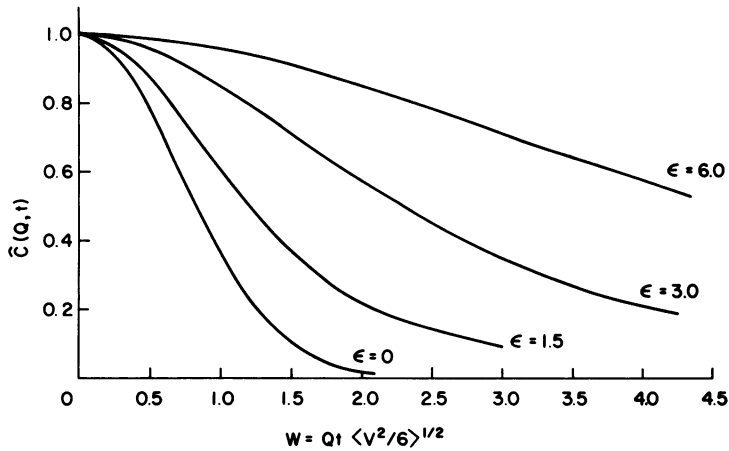
FIGURE 2 Normalized autocorrelation functions for motile ellipsoidal "Gaussian particles," calculated according to Eq. 13. The parameter ϵ is given as $\epsilon = [(L^2 - w^2)/10]^{1/2}Q$, where L and w are the major and minor axes of the particles, and Q is the Bragg wave vector (see Eq. 14). In a typical experiment ϵ would change in proportion to Q, the latter arising from changes in the scattering angle.

As shown in Appendix C, Eqs. 9 and 11 lead to the simple result

$$\hat{C}(Q, t) = \{[\mathrm{erf}(\epsilon z)/z] + (2/\sqrt{\pi})(z^2 - 1)e^{-z^2\epsilon^2}\}/z^2\,\mathrm{erf}\,\epsilon, \tag{13}$$

where the parameters ϵ and z are defined as

$$\epsilon = Q(\sigma_\parallel^2 - \sigma_\perp^2)^{1/2}$$

$$z = \{1 + t^2\langle V^2/6\rangle Q^2/\epsilon^2\}^{1/2} \tag{14}$$

$$\equiv \{1 + W^2/\epsilon^2\}^{1/2} \tag{15}$$

and $\mathrm{erf}(y) = 2/\sqrt{\pi}\int_0^y \exp(-x)dx$ is the "error function" whose values are tabulated (14). Correlation functions computed from this expression are shown in Fig. 2, results being plotted in terms of the reduced variable $W = Qt\langle V^2/6\rangle^{1/2}$ and parametrized by ϵ (cf. Eq. 14). Note that, for a He-Ne laser, $Q \sim 10^5 \mathrm{cm}^{-1}$ when the scattering angle is 45°. Thus, for a particle whose length is $\sim 1.2\ \mu$m and width is $\sim 0.4\ \mu$m (the approximate body dimensions of a moderately sized *E. coli* bacterium) one finds (with $\sigma_\parallel = L/\sqrt{10}$) that $\epsilon \simeq 3.6$. This puts us well within the range where significant deviations from the ideal Qt scaling relationship expressed by Eq. 10 would be predicted.

However, with regard to measurements on *E. coli* bacteria, we caution that this simple model probably is not directly applicable since it implicitly represents the bacteria as rod-shaped microorganisms of uniform optical polarizability. In fact, phase contrast microscopy shows internal structures ("chromatinic bodies") which occupy only

part of the cell volume (7, 8). Thus, the effective size of the bacteria may be somewhat smaller than the geometrical size as far as light scattering is concerned (15, 16). This point is further discussed in Secs. V and VI, where we investigate models of optically heterogeneous microorganisms.

In general, if the Qt scaling relationship is not observed experimentally, it is difficult to extract swimming speed distributions from $C(Q, t)$. In such case the structure of the microorganism needs to be specified with considerable precision in order that unambiguous values of the motility parameters be obtained. On the other hand, Eqs. 13 and 15 indicate that the spectra are functionals of $\langle V^2 \rangle^{1/2} t$. Thus, by performing measurements at a fixed scattering angle, relative values of swimming speed can be determined even when Eq. 10 is not applicable.

IV. DIFFUSING PARTICLES

The Gaussian mass model also can be used to investigate the manner in which interference scattering might affect spectra obtained for large freely diffusing particles (for example, bacteria whose metabolism has been inhibited [17]). For sufficiently large particles, rotational diffusion times are very long compared with translational diffusion times, so that in Eq. 7 $\mathbf{u}(t)$ can be approximated as a stationary quantity. Thus, Eq. 7 becomes

$$C(Q, t) = \langle \exp(i\mathbf{Q} \cdot \Delta \mathbf{R}(t)) \exp(-\Delta \sigma^2 Q^2 [\hat{\mathbf{Q}} \cdot \mathbf{u}]^2) \rangle. \tag{16}$$

To evaluate Eq. 16 we first average over the translational motion, keeping the particle orientation fixed, viz.,

$$\langle \exp(i\mathbf{Q} \cdot \Delta \mathbf{R}(t)) \rangle_{\text{fixed } \mathbf{u}} = \exp(-\mathbf{Q} \cdot \mathbf{D} \cdot \mathbf{Q}t), \tag{17}$$

where the translational diffusion tensor is

$$\mathbf{D} = D_{\parallel} \mathbf{u}\mathbf{u} + D_{\perp}(\mathbf{I} - \mathbf{u}\mathbf{u}). \tag{18}$$

Here, $D_{\parallel}$ and $D_{\perp}$ are the translational diffusion coefficients for motions parallel and perpendicular to $\mathbf{u}$, respectively, and $\mathbf{I}$ is the unit tensor.

Substituting these results into Eq. 16 gives

$$\begin{aligned}
C(\mathbf{Q}, t) &= \exp(-Q^2 D_{\perp} t) \langle \exp(-[\Delta \sigma^2 + (D_{\parallel} - D_{\perp})t](\mathbf{Q} \cdot \mathbf{u})^2) \rangle \\
&= \exp(-Q^2 D_{\perp} t) \int_{-1}^{1} (d\eta/2) \exp(-[\Delta \sigma^2 + (D_{\parallel} - D_{\perp})t] Q^2 \eta^2)
\end{aligned} \tag{19}$$

where $\eta = \mathbf{Q} \cdot \mathbf{u} / |\mathbf{Q}|$ again is the cosine of the angle between $\mathbf{Q}$ and $\mathbf{u}$. Alternatively, the correlation function can be normalized and expressed in terms of error func-

tions as

$$\hat{C}(Q, t) = \frac{e^{-Y}}{[1 + \psi Y]^{1/2}} \frac{\mathrm{erf}[\epsilon(1 + \psi Y)^{1/2}]}{\mathrm{erf}[\epsilon]} \tag{20}$$

where ϵ is defined in Eq. 14 and Y and ψ are defined as

$$Y \equiv D_\perp Q^2 t \tag{21}$$

$$\psi \equiv (D_\parallel - D_\perp)/(\sigma_\parallel^2 - \sigma_\perp^2) D_\perp Q^2. \tag{22}$$

This result reduces to $\exp(-Q^2 Dt)$ for a sphere.

It should be noted that in general the correlation function does not scale with $Q^2 Dt$ as it does for a sphere. Interestingly, however, for large particles the deviations from scaling are small. For example, for *E. coli,* one expects $(D_\parallel - D_\perp) \sim \mathcal{O}(10^{-9}\,\mathrm{cm^2/s})$, $(\sigma_\parallel^2 - \sigma_\perp^2) \sim \mathcal{O}(10^{-8}\,\mathrm{cm^2})$, $t \lesssim \mathcal{O}(10^{-2}\,\mathrm{s})$, so that $\psi Y < \mathcal{O}(10^{-2})$ in Eq. 20. Consequently, nonscaling corrections to $\hat{C}(Q, t)$ are predicted to be small in this case, in agreement with experimental observations (17).

V. INTERNALLY STRUCTURED PARTICLES

Gross geometric shape may not be the best representation of the structure of a microorganism for the purpose of computing light-scattering spectra. Viruses and cells are inhomogeneous, and their constituent materials have differing optical properties. Since the intensity of the light scattered by a structure is proportional to the difference between the optical polarizability of the structure and that of the surrounding material, the light scattering spectrum may in fact depend primarily on those parts of the microorganism whose index of refraction is very different from that of the culture medium.

For example, bacteria contain nuclear figures (chromatinic bodies) which are composed of material of relatively low refractive index. These regions show up clearly in investigations, by phase contrast microscopy, of dividing cultures of *E. coli.* One or more (usually two) distinct bodies are observed, and their somewhat irregular morphology changes as the bacteria grow and divide (8). The significant point, however, is that the chromatinic bodies are considerably smaller and, when averaged over all orientations, more nearly spherical than are the bacteria themselves. The proportion of multinucleate to uninucleate cells depends on culture conditions. When the bacteria are vegetative—for example, when suspended in a buffered motility medium which does not support growth—almost all members of the culture contain only one chromatinic body lying near the center of the cell. On the other hand, when the bacteria are rapidly growing, the chromatinic bodies usually are visualized in pairs, localized at the ends of each cell (8).

We now analyze a shell-like model meant to represent uninucleate cells. We suppose that the particle of interest consists of an *interior* ellipsoidal region, containing scattering centers having excess polarizability $\tilde{a}$, and an *exterior* region composed of scatter-

ing centers having excess polarizability a. The correlation function for this type of particle may be calculated as in Sec. II except that, in place of Eq. 2, we now have

$$C(Q,t) = \langle e^{i\mathbf{Q}\cdot\Delta\mathbf{R}(t)} \mid S_a(\mathbf{Q},t,\mathbf{u}) \mid^2 \rangle, \tag{23}$$

where $S_a(\mathbf{Q},t,\mathbf{u})$ is here given as

$$S_a(\mathbf{Q},t,\mathbf{u}) = a \sum_{\substack{\text{Entire}\\\text{particle}}} e^{i\mathbf{Q}\cdot\rho_i} + (\tilde{a} - a) \sum_{\substack{\text{Interior}\\\text{region}}} e^{i\mathbf{Q}\cdot\rho_i}. \tag{24}$$

Thus, after again invoking the Gaussian model for each sum in Eq. 24 we find that $S_a(\mathbf{Q},t,\mathbf{u})$ is given as (cf. Eqs. 3, 5–7)

$$S_a(\mathbf{Q},t,\mathbf{u}) = Na \exp\left(-\frac{\sigma_\perp^2}{2}Q^2\right)\exp\left(-\frac{\Delta\sigma^2}{2}[\mathbf{Q}\cdot\mathbf{u}]^2\right)$$
$$+ \tilde{N}(\tilde{a} - a)\exp\left(-\frac{\tilde{\sigma}_\perp^2 Q^2}{2}\right)\exp\left(-\frac{\Delta\tilde{\sigma}^2}{2}[\mathbf{Q}\cdot\mathbf{u}]^2\right), \tag{25}$$

where N represents the total number of scattering centers, and $\tilde{N}$ the number of scattering centers in the interior ellipsoid. The parameters $\sigma_\perp$ and $\Delta\sigma$ relate to the overall dimensions of the particle, whereas $\tilde{\sigma}_\perp$, $\Delta\tilde{\sigma}$ relate to the dimensions of the smaller interior.

The function $\mid S_a(\mathbf{Q},t,\mathbf{u}) \mid^2$ in Eq. 23 contains four terms, each having a form equivalent to that which appears in Eq. 7. Thus, the techniques used in Sec. III could be used to determine $\hat{C}(Q,t)$ for the current model. However, even without performing the computations, we observe that the light-scattering spectrum of a large particle may depend more on the morphology and motions of internal organelles than on the dimensions and movements of the particle as a whole. In effect, the light-scattering structure of a biological cell depends both on the index of refraction of its constituents and, also, on the manner by which interference scattering leads to reduced scattering intensities from the different regions.

These points are illustrated if Eq. 23 is analyzed for a model bacterium. We first note that when the index of refraction of the culture medium is adjusted to be close to that of the exterior region of the cell, then $a = 0$, and only the smaller interior is visible. This technique has been used to visualize the morphologic changes of chromatinic bodies which accompany cell division (8). However, when the suspending medium has an index of refraction close to that of water, the factors a and $(\tilde{a} - a)$ are comparable.[3] In this case, the dominant influence on the light-scattering spectrum is the shape and size of the cell organelles.

---

[3]Cross and Latimer (16) have explained the angular dependence of total intensity scattering spectra of *E. coli* by choosing the refractive index of the exterior portion of the cell to be 1.10 times that of water (the suspending medium) and the relative refractive index of the interior material to be 1.045. Wyatt (18) has employed similar values for his studies of light scattered by various bacterial suspensions.

Thus, in Eq. 23 we see that the factors $\exp(-\sigma_\perp Q^2/2)$, $\exp(-\tilde{\sigma}_\perp Q^2/2)$ act to attenuate the intensity of the scattered field. For *E. coli,* the product $\sigma_\perp Q$ is of the order of 10 at moderate (i.e. not very small) scattering angles. Since $\sigma_\perp Q$ and $\tilde{\sigma}_\perp Q$ appear as exponential factors, even a 20% difference between $\sigma_\perp$ and $\tilde{\sigma}_\perp$ (these being proportional, respectively, to the exterior and interior dimensions of the scattering regions) markedly increases the relative importance of scattering from the interior region. Similarly, the terms $\Delta\sigma^2$, $\Delta\tilde{\sigma}^2$ influence the spectrum in the same way, except that, additionally, anisotropy is important. For example, if the interior region is spherical, one finds that $\exp(-\frac{1}{2}\Delta\tilde{\sigma}^2) = 1$, whereas the analogous term $\exp(-\frac{1}{2}\Delta\sigma^2)$ can be quite small. Although the total number of scattering centers N exceeds those in the interior region $\tilde{N}$, the attenuation factors due to structure are generally more significant in determining relative scattering intensity.

Due to their irregular shapes and due, also, to the fact that their orientation within the cells seems to be variable, it is difficult to specify the dimensions of the chromatinic bodies of *E. coli* with great precision. However, on the average l seems to be greater than w, values of $l \simeq 0.8 \mu$m, $w \simeq 0.6 \mu$m perhaps being typical (7, 8). The value of ϵ which corresponds to these dimensions at, e.g., a scattering angle of 45°, is $\epsilon \simeq 1.7$. By contrast, if the overall cell dimensions of $L = 1.5 \mu$m, $w = 0.8 \mu$m were to be used, ϵ would have the value $\epsilon = 4$. Thus, a significant reduction in effective size is achieved, which has the effect of squeezing the theoretical spectra given by Eq. 13 into a rather narrow range lying relatively close to the $\epsilon = 0$ limit (see Fig. 2).

Even so, the predicted variance from Qt scaling exceeds that which has been observed experimentally (12). This might be due to an overestimate, here, of the anisotrophy of the chromatinic bodies, particularly insofar as we have neglected off-axial particle orientations (see Appendix B). On the other hand, nonmotile contaminants possibly present in a sample would give spectral components having nonscaling characteristics opposite to those shown in Fig. 2; when plotted as a function of Qt, such spectra decay more rapidly at successively higher values of Q. The presence of such contaminants could lead to spurious demonstrations of Qt scaling under certain conditions.

VI. DUMBBELL-SHAPED SCATTERERS

Another structured particle which is easily analyzed in terms of the procedures developed in Secs. II–III is an ellipsoidal dumbbell. This model is suggested by the visualization of dual chromatinic bodies in proliferating bacteria.

We now treat the scattering region as being composed of two linked identical ellipsoids of revolution, having length l and width w, and separated by a constant distance d. Following along the lines which led to Eq. 7 we find, for this geometry,

$$C_{db}(Q, t) = a_N^2 e^{-\sigma_\perp^2 Q^2} \left\langle e^{iQ\cdot\Delta R(t)} \cos^2\left(\frac{Qd}{2}[\hat{Q}\cdot u]\right) e^{-\Delta\sigma^2 Q^2[\hat{Q}\cdot u]} \right\rangle . \tag{26}$$

Here, $\Delta\sigma^2$ has the same form as that previously given (cf. Eq. 7 ff. and Eq. 5) but the
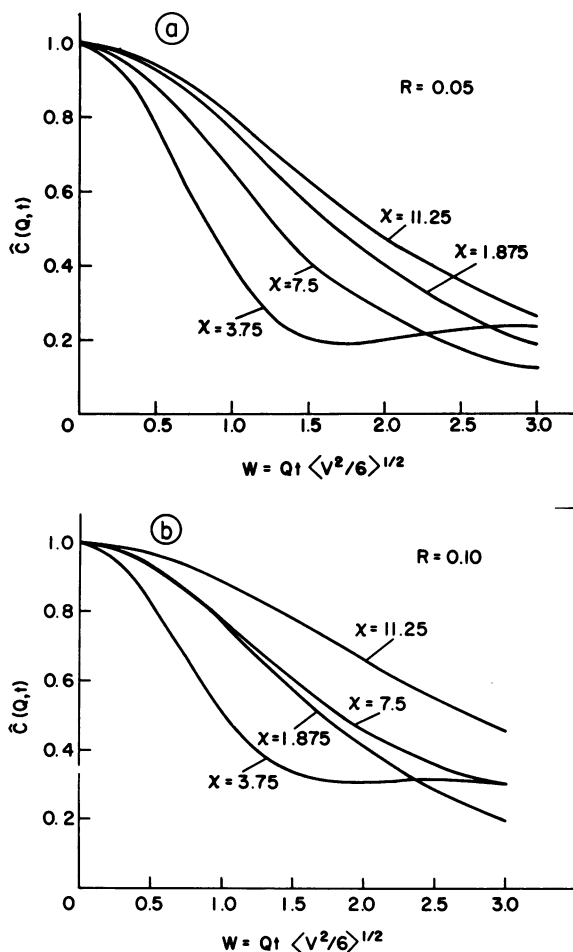
FIGURE 3 Normalized autocorrelation functions for motile ellipsoidal dumbbells, calculated according to Eq. 27. The parameters χ and R are defined as $\chi = Qd/2$, $R = \epsilon^2/\chi^2 = 4\Delta\sigma^2/d^2$, where $\Delta\sigma^2$ pertains to the dimensions of the dumbbell sections (e.g., $\Delta\sigma^2 = (l^2 - w^2)/10$), and d is the distance between the two dumbbell centers. If d is taken to be 1.5 μm, a scattering angle of 45° implies $\chi \simeq 7.5(\lambda = 6,328 \text{ Å})$. (a) $R = 0.05$, corresponding to, e.g., $l = 0.8$ μm, $w = 0.6$ μm, $d = 1.5$ μm. (b) $R = 0.10$.

effective length of the scattering region now is that of the smaller optically distinct portions of the cell (i.e. the dumbbell sections), rather than being the overall cell length. Since the lengths of these regions are similar to their widths, the effects of asymmetry are mitigated (see, also, the discussion of the previous section).

Due to the $\cos^2(Qd\eta/2)$ term, we have not been able to obtain an analytic reduction of Eq. 26 similar to Eq. 13. However, upon proceeding as with Eqs. 7–9 but interchanging the V and η integrations, we find

$$\hat{C}_{db}(Q,t) = \frac{\int_{-1}^{1} e^{-\epsilon^2 y^2} \cos^2 \chi y e^{-y^2 W^2} [1 - 2W^2 y^2] dy}{\int_{-1}^{1} e^{-\epsilon^2 y^2} \cos^2 \chi y \, dy}, \qquad (27)$$

where ϵ and W have the definitions given in Eqs. 14 and 15. The parameter χ is defined as

$$\chi = Qd/2. \qquad (28)$$

Note that in the limit $\chi \gg 1$ the term $\cos^2 (\chi y)$ varies rapidly about its average value and can be approximated as $\cos^2 (\chi y) = 0.5[1 - \cos 2\chi y] \approx 0.5$ (i.e. the integral over the varying part is small compared with the integral over the constant). Consequently, in such limit we get an expression which represents scattering from optically noninterfering dumbbells of relatively small dimension (cf. Eq. 13). However, in general the integral in Eq. 27 needs to be performed numerically, but this can be accomplished without much difficulty.

Representative results are shown in Fig. 3. The most notable aspect of these curves is the extent to which they overlap, particularly when compared with those shown in Fig. 2. A certain amount of Q-dependent dispersion arises due to the large distance between the dumbbells (see Fig. 3 b). However, the smaller size and decreased anisotropy of the scattering structures leads to a net increase in the degree by which the correlation functions approach the scaling relationship expressed by Eq. 10.

REFERENCES

1. CUMMINS, H. Z., F. D. CARLSON, T. J. HERBERT, and G. WOODS. Biophys. J. 1969. 9:518.
2. DUBIN, S. B., G. B. BENEDEK, F. C. BANCROFT, and D. FREIFELDER. 1971. J. Mol. Biol. 54:547.
3. PUSEY, P. N., D. W. SCHAEFER, D. E. KOPPEL, R. D. CAMERINI-OTERO, and R. M. FRANKLIN. 1972. J. Phys. (Paris). 33:C1-33.
4. UZGIRIS, E. E. 1972. Opt. Commun. 6:55.
5. NOSSAL, R., and S. H. CHEN. 1973. Nat. New Biol. 244:253.
6. SCHAEFER, D. W., G. BANKS, and S. ALPERT. 1974. Nature (Lond.). 248:162.
7. STEMPEN, H. 1950. J. Bacteriol. 60:81.
8. MASON, D. J., and D. M. POWELSON. 1956. J. Bacteriol. 71:474.
9. PECORA, R. J. Chem. Phys. 1968. 48:4126.
10. BERNE, B., and R. PECORA. 1975. Dynamic Light Scattering in Chemistry, Physics, and Biology. John Wiley & Sons, Inc., New York. In press.
11. FEINLEIB, M. E., and G. M. CURRY. 1971. Physiol. Plant. 25:346.
12. NOSSAL, R., S. H. CHEN, and C. C. LAI. 1971. Opt. Commun. 4:35.
13. BOON, J. P., R. NOSSAL, and S. H. CHEN. 1974. Biophys. J. 14:000.
14. ABRAMOWITZ, M., and I. A. STEGUN. 1964. Handbook of Mathematical Functions. National Bureau of Standards, Washington, D.C.
15. KOCH, A. L., and E. EHRENFELD. 1968. Biochem. Biophys. Acta. 165:262.
16. CROSS, D. A., and P. LATIMER. 1972. Appl. Opt. 11:1225.
17. NOSSAL, R., and S. H. CHEN. 1972. J. Phys. (Paris). 33:C1-171.

18. Wyatt, P. J. 1972. *J. Colloid Interface Sci.* **39**:479.
19. Holtzer, A. M. 1955. *J. Polymer Sci.* **17**:432.

APPENDIX A: SCATTERING FROM INFINITELY THIN MOTILE RODS

We now compute the correlation function $C(Q, t)$ pertaining to an infinitely thin rod of length L. By fitting the results to those for the Gaussian model (Eq. 5 ff.) we can relate the widths $\sigma_{\parallel}$, $\sigma_{\perp}$ of the Gaussian mass distribution to the actual cell boundaries.

We divide the rod into N segments and designate y_j as the position of the jth segment taken with respect to the center of mass. In place of Eq. 2 we now have

$$C(\mathbf{Q}, t) = a_N^2 \left\langle e^{i\mathbf{Q} \cdot \Delta \mathbf{R}(t)} \frac{1}{N} \sum_{j=1}^{N} e^{+i\mathbf{Q} \cdot \mathbf{u}(t) y_j} \cdot \frac{1}{N} \sum_{k=1}^{N} e^{-i\mathbf{Q} \cdot \mathbf{u}(0) y_k} \right\rangle . \qquad (29)$$

Taking the limit $N \longrightarrow \infty$ provides

$$\frac{1}{N} \sum_{j=1}^{N} e^{i\mathbf{Q} \cdot \mathbf{u}(t) y_j} = \int_{-L/2}^{L/2} \frac{dy}{L} e^{i\mathbf{Q} \cdot \mathbf{u}(t) y} = j_0(\mathbf{Q} \cdot \mathbf{u}(t) L/2),$$

where $j_0(z) = \sin(z)/z$ is the spherical Bessel function of order zero. Thus, again presuming that the particle always moves parallel to its long axis, we find from Eq. 29 (cf. Eq. 9)

$$C_{\text{rod}}(Q, t) = a_N^2 \left\langle e^{i\mathbf{Q} \cdot \Delta \mathbf{R}(t)} \mid j_0(\mathbf{Q} \cdot \mathbf{u}(0) L/2) \mid^2 \right\rangle \qquad (30)$$

$$= \frac{a_N^2}{2} \int_0^{\infty} dV \int_{-1}^{1} d\eta \, e^{iQV t \eta} \mid j_0\left(\frac{QL}{2} \eta\right) \mid^2 W(V). \qquad (31)$$

When the speed distribution represented by Eq. 11 is used in Eq. 31, the V integrations can be achieved without difficulty. Subsequently, after some straightforward manipulation the normalized correlation function can be expressed as

$$\hat{C}_{\text{rod}}(Q, t) = \frac{\dfrac{1}{2\zeta} \displaystyle\int_{-\zeta}^{\zeta} dy \mid j_0(y) \mid^2 e^{-W^2 y^2/\zeta^2}[1 - 2y^2 W^2/\zeta^2]}{\dfrac{1}{2\zeta} \displaystyle\int_{-\zeta}^{\zeta} dy \mid j_0(y) \mid^2}, \qquad (32)$$

where W and ζ are defined as

$$W \equiv Q \langle V^2/6 \rangle^{1/2} t; \quad \zeta \equiv QL/2. \qquad (33)$$

In Fig. 4 we show $\hat{C}_{\text{rod}}(Q, t)$ for two different values of ζ. For comparison, we have set $\sigma_{\perp} = 0$ in Eq. 13, and have varied $\sigma_{\parallel}$ to achieve good correspondence between the $\hat{C}(Q, t)$ of the two models. We see that the correlation functions virtually superimpose when $\sigma_{\parallel}$ is chosen to be $\sigma_{\parallel} = L/\sqrt{10}$.
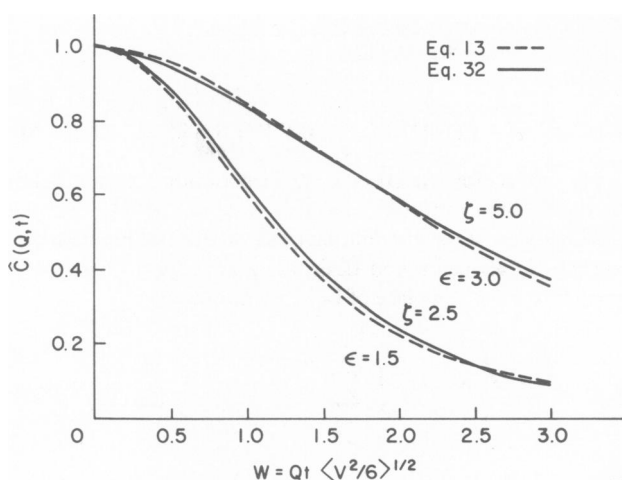
FIGURE 4 Comparison between autocorrelation functions for motile thin rods (Eq. 32) and motile Gaussian ellipsoids (Eq. 13) with $\sigma_\perp = 0$. Good correspondence is achieved when $\sigma_\parallel$ is taken to be $\sigma_\parallel = L/\sqrt{10}$, where L is the length of the rod.

APPENDIX B: EFFECTS OF OFF-AXIAL ORIENTATION

In Secs. II-VII we consistently presumed that the particles move in directions parallel to their major axes. Although this assumption is correct for the average orientation, in reality there is some dispersion about this idealized directional ordering. For example, for certain culture conditions or particular strains of *E. coli,* wiggling movements are present, so that at any given moment a number of bacteria are oriented such that their long axes lie obliquely with respect to their directions of translational motion (13). Such off-axial orientation diminishes the degree to which particle anisotropy causes deviations from the Qt scaling relation expressed by Eq. 10.

This may be illustrated by extending the calculation of $\hat{C}_{\mathrm{rod}}(Q,t)$ previously outlined in Appendix A. As before, we let $\hat{u}$ be a unit vector lying along the major axis of the particle. Also, we define α as the angle between $\hat{u}$ and the direction of motion, V. We now find it convenient to fix the x axis to be directed along V and take the y axis as lying in the plane defined by $\hat{u}, V$. We then average over all possible orientations of Q relative to these axes (see also ref. 13).

The components of $V, \hat{u},$ and Q are thus given as

$$V = \{V, 0, 0\}$$
$$\hat{u} = \{\cos\alpha, \sin\alpha, 0\} \tag{34}$$
$$Q = \{Q\sin\theta\cos\varphi, Q\sin\theta\sin\varphi, Q\cos\theta\}$$

where θ is the angle between Q and the z axis, and φ is the angle between x and the projection of Q on the $\{x, y\}$ plane. When Eq. 30 is expressed as

$$C(Q,t) = \frac{a_N^2}{L^2} \int_{-L/2}^{L/2} dy \int_{-L/2}^{L/2} dz \left\langle e^{iQ\cdot Vt} e^{i(y-z)Q\cdot\hat{u}} \right\rangle \tag{35}$$

then, using Eq. 34, we have

$$C(Q,t) = \frac{a_N^2}{L^2} \int_{-L/2}^{L/2} dy \int_{-L/2}^{L/2} dz \int_0^\infty dV\, W(V) \cdot \left\langle \frac{1}{4\pi} \int_0^\pi d\theta \sin\theta \int_0^\pi d\varphi \right.$$

$$\left. \cdot \exp(i\varphi\,\sin\theta\{(Vt + [y - z]\cos\alpha)\cos\varphi + [y - z]\sin\alpha\sin\varphi\}) \right\rangle, \quad (36)$$

where the brackets $\langle \ldots \rangle$ here signify averaging with respect to the angle of inclination α. The integrals over θ and φ can be performed (13), so that Eq. 36 becomes.

$$C(Q,t) = \frac{a_N^2}{L^2} \int_{-L/2}^{L/2} dy \int_{-L/2}^{L/2} dz \int_0^\infty dV$$

$$\cdot W(V)\, \langle j_0(Q[(Vt)^2 + 2(y - z)Vt\cos\alpha + (y - z)^2]^{1/2}) \rangle. \quad (37)$$

Thus, upon expanding the Bessel function according to (14) $j_0((\rho^2 + r^2 - 2\rho r\cos\theta)^{1/2}) = \sum_{n=0}^\infty (2n + 1)j_n(\rho)j_n(r)P_n(\cos\theta)$ where the $P_n(\cdots)$ are Legendre polynomials, we can express Eq. 37 as

$$C(Q,t) = a_N^2 \sum_{n=0}^\infty (4n + 1) B_{2n}(QL) \cdot \int_0^\infty dV\, W(V)j_{2n}(QVt) \cdot \langle P_{2n}(\cos\alpha) \rangle, \quad (38)$$

where the $\{B_k(QL)\}$ are defined as

$$B_k(QL) \equiv L^{-2} \int_{-L/2}^{L/2} dy \int_{-L/2}^{L/2} dz\, j_k(Q(y - z)). \quad (39)$$

Note that, since $j_k(z) = -j_k(-z)$, $k = 1, 3, 5 \ldots$, one finds $B_k = 0$ if k is odd. (Thus, only terms of even order appear in Eq. 38. When the particles are aligned along the directions of their translational motion, $\alpha = 0$ and $\langle P_{2n}(\cos\alpha) \rangle = 1$ for all n.

The $\{B_k\}$ are easily expressed in terms of familiar functions. For example, we find

$$B_0(x) = (2/x)\{\text{Si}(x) + ([\cos x - 1]/x)\} \quad (40)$$

and

$$B_2(x) = (1/x)\{\text{Si}(x) - 3j_1(x)\} + (2/x^2)\{3j_0(x) - \cos x - 2\}, \quad (41)$$

where $\text{Si}(\cdots)$ is the Sine integral and is tabulated (14). The expression given by Eq. 40 is the structure factor which appears in theories of classical light scattering from hard rods (19). The ratio $S_2(x) \equiv B_2(x)/B_0(x)$ is shown in Fig. 5. It rises markedly over the range $0 \leq x \leq 8$, after which it attains a more-or-less constant plateau value of approximately 0.4. Since $\langle j_2(QVt) \rangle / \langle j_0(QVt) \rangle$ also has a value of approximately 0.3–0.4 at the half-decay point of $C(Q, t)$ (13), Eq. 38 indicates that the first correction term (i.e., that proportional to $\langle j_2(QVt) \rangle$) can be quite significant when compared with the zeroth order term given by Eq. 10 (i.e., that proportional to $\langle j_0(QVt) \rangle$). This conclusion is consistent with the results shown in Fig. 4 regarding the non-scaling of $\hat{C}_{\text{rod}}(Q, t)$.
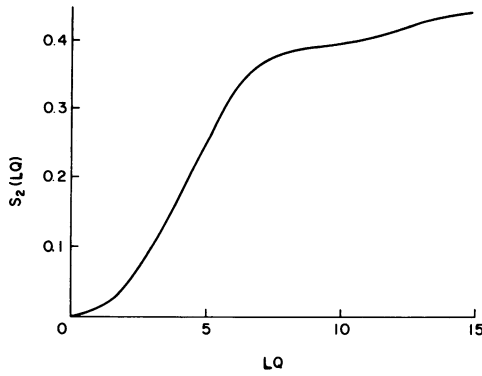
FIGURE 5 The ratio $B_2(QL)/B_0(QL)$, calculated according to Eqs. 40 and 41.

To what extent can off-axial orientations reduce the relative magnitudes of the higher order terms in the expansion given by Eq. 38? We need to know the distribution of orientation angles $P(\cos\alpha)$ in order to calculate the factors $\langle P_\eta(\cos\alpha)\rangle$. An estimate can be obtained if we choose the following distribution

$$P(\cos\alpha)d\cos\alpha = \begin{cases} 1/(2 - 2\cos\alpha_m) & \text{if } 1 \geq \cos\alpha \geq \cos\alpha_m \\ 0 & \text{if } \cos\alpha < \cos\alpha_m. \end{cases} \quad (42)$$

From Eq. 42 we find

$$\langle P_2(\cos\alpha)\rangle = [\cos\alpha_m(1 + \cos\alpha_m)]/2. \quad (43)$$

If the maximum angle α_m is taken to be 30°, Eq. 43 yields $\langle P_2\rangle \simeq 0.83$; if α_m is 45°, then $\langle P_2\rangle$ is reduced to 0.6. These results suggest that, although off-axis orientations will indeed reduce the degree to which $\hat{C}(Q, t)$ deviates from the "ideal" Qt scaling expressed by Eq. 1, they cannot entirely account for the close approximation to scaling previously reported for measurements of light scattered by E. coli (12).

APPENDIX C: DERIVATION OF EQ. 13

Combining Eqs. 9 and 11 and changing the orders of integration yields

$$\hat{C}(Q,t) = \frac{2\gamma^3}{\sqrt{\pi}} \int_{-1}^{1} d\eta\, e^{-\Delta\sigma^2 Q^2\eta^2} \int_{0}^{\infty} dV\{V^2 e^{-\gamma^2 V^2} \cos(QVt\eta)\} \quad (44)$$

$$= -\frac{\gamma^2}{\sqrt{\pi}} \cdot \frac{d}{d\gamma} \int_{-1}^{1} d\eta\, e^{-\Delta\sigma^2 Q^2\eta^2} \left\{\frac{\sqrt{\pi}}{2\gamma} e^{-Q^2\eta^2 t^2/4\gamma^2}\right\} \quad (45)$$

$$= -\frac{\gamma^2\sqrt{\pi}}{Q} \cdot \frac{d}{d\gamma} \left\{\frac{1}{(4\gamma^2\Delta\sigma^2 + t^2)^{1/2}} \text{erf}(Q(\Delta\sigma^2 + t^2/4\gamma^2)^{1/2})\right\}. \quad (46)$$

Thus, upon taking the derivatives with respect to γ in Eq. 46 and substituting according to Eqs. 14, 15, and 12, one obtains the expression given by Eq. 13.